Heliyon 10 (2024) e30824

Contents lists available at ScienceDirect

Heliyon

journal homepage: www.cell.com/heliyon

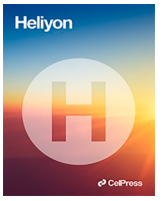

Research article

Nano cells from fruit bunch residue: Nestling nanotechnology within the circular oil palm milling residue management

Arniza Ghazali [a,*], Nur Haffizah Azhar [a], Rabeta Mohd Salleh [b], Mohd Rafatullah [c], Melati Khairuddean [d], Shahrom Mahmud [e]

[a] Division of Bioresource Technology, School of Industrial Technology, Universiti Sains Malaysia, 11800, USM, Penang, Malaysia
[b] Department of Community Health, Advanced Medical and Dental Institute, Universiti Sains Malaysia, 13200, USM Bertam, Penang, Malaysia
[c] Division of Environmental Technology, School of Industrial Technology, Universiti Sains Malaysia, 11800, USM, Penang, Malaysia
[d] School of Chemical Sciences, Universiti Sains Malaysia, 11800, USM, Penang, Malaysia
[e] Nano-Optoelectronic Research and Technology (NOR) Lab, School of Physics, Universiti Sains Malaysia, 11800, USM, Penang, Malaysia

ARTICLE INFO

Keywords:
EFB
Alkaline peroxide
Dioxydanyl radical
Circularity
Delamination
Nano-functional
Biomass

ABSTRACT

Nano-structured materials gain a vast market acceptance mainly due to their overarching endurance. Nanofibrillar cellulose (NFC) is one example of an augmenting agent unviable for production by small and medium enterprises (SMEs) due to the underlying process complexity. This study aims to characterise the NFC-alternative cells denoted as TRX-cells®, which is a mix of cellulose and non-cellulose components, ruling out its status as 'cellulose nanofibers, CNF'. The aim to test-fit the TRX-cells® production process into the circularity model was executed by deliberating on the usability of the byproduct. In doing so, fibrous oil palm empty fruit bunch (EFB) was treated with dioxydanyl radicals (DIOR) and homogenised. The rapid EFB-DIOR reaction at 70°C targeting dearomatisation reaction in a 10%-solid open system was performed before refining the DIOR-treated EFB to micro-scale fibres. Subjecting the micro-fibres to 17 kWh/mt PFI-milling yielded 85–95% of nano-scale fibrous mass. Relative to the stiff micro-fibres, the nano-scale cells web exhibit 34–41% softness enhancement judged from the web tear resistance profile associated with inter-fibre space reduction. Advanced chromatographic evidence for 27% xylan amongst TRX-cells® total aldo-sugars was one form of the non-cellulose nano-component. High-resolution Transmission Electron Microscopy hyphenated to Energy Dispersive Analysis of X-ray (HRTEM-EDX) elemental mapping showed a 0.4 atomic percentage of nano-biominerals, confirming the presence of the redistributed dearomatised cells adjacent to cellulose held in the web of the hemicellulose. Shearing at the dearomatised inter-cell wall layers by PFI mill peeled 5 nm–100 nm thickness laminae. The smorgasbord of cellulose and non-celluloses resulted in crystallinity comparable to softwood NFC of approximately 60%, with unique preservation and precision-printing enabling properties. Given the non-recyclability of the DIOR-treated EFB microfibres, nestling the rapid waste transformation process into the circularity model shed light on circular bio-nanotechnology to the spectrum of opportunity for zero-waste, reduced emission and net zero carbon practices on top of an added value from waste transformation to a product.

* Corresponding author.
E-mail address: arniza@usm.my (A. Ghazali).

https://doi.org/10.1016/j.heliyon.2024.e30824
Received 12 December 2023; Received in revised form 20 April 2024; Accepted 6 May 2024
Available online 9 May 2024

1. Introduction

1.1. Oil palm residue circular management

With the prolonged conflicts between the world's sunflower oil producers, palm oil suppliers remain in solidarity to protract a smooth global edible oil supply as an economic substitute [1,2] while preventing aggravation of the food crisis. The food oil supply is also projected to surge with the current rising demand from newly booming nations like India [3], in addition to the outpouring of the global population [4–6]. Alongside the enormous multi-billion-dollar supply of oil for global needs [7,8] comes the fibrous fruit bunch residues housing various forms of commodities. Cellulose, extractives and lignin are the often-referenced commodities (Fig. 1) besides the hidden and less said flavours, pigments, therapeutics and countless others.

Deliberation on the fruit bunch fibrous residues brought about enormous research on the remnant's potential uses with briquette, animal feed, fertilisers and biofuel [16–18] already in the industry's integrated business model. Due to the ensuing high-capital and high-scale operational demand required of nanomaterials manufacturing, the advanced OPR (oil palm residues) transformation to the nanoscale functional materials needs clear-sighted planning to avoid resource-intensiveness.

1.2. Nano cellulose and EFB-nanotechnology attraction

Economic pure cellulose extraction [19,20] unfolded the numerous chlorine-based systems [21–23] that yield pure cellulose fibres, and consequently low yield. While chlorine-related operation systems [19,20] are only scanty, sulfur-based fibre extraction process [24,25], may be more superior from yield perspectives. The revived sulfur-based systems like the Magnefite process that evolved with an efficient resource recovery can be smartly designed to reroute wastes such as fines to nanocellulose production [25]. Conversion of wastes to monetary values is recommended to leverage the extra capital underpinning the stringent 'cleansing' requirements to curb the corrosive emissions and discharge treatment. Some of these and other alkali techniques have also been proven successful in purifying cellulose from the oil palm empty fruit bunches (EFB) [20,21,26–28] at the laboratory scale. Nanocellulose and nano-whiskers at less than 50% yield was possibly generated, all of which are characterised by the nanometre scale diameter of the fibrils [28–30].

The year-round abundant EFB prompted astounding research on nanofibrillar cellulose (NFC) and microfibrillated cellulose (MFC)

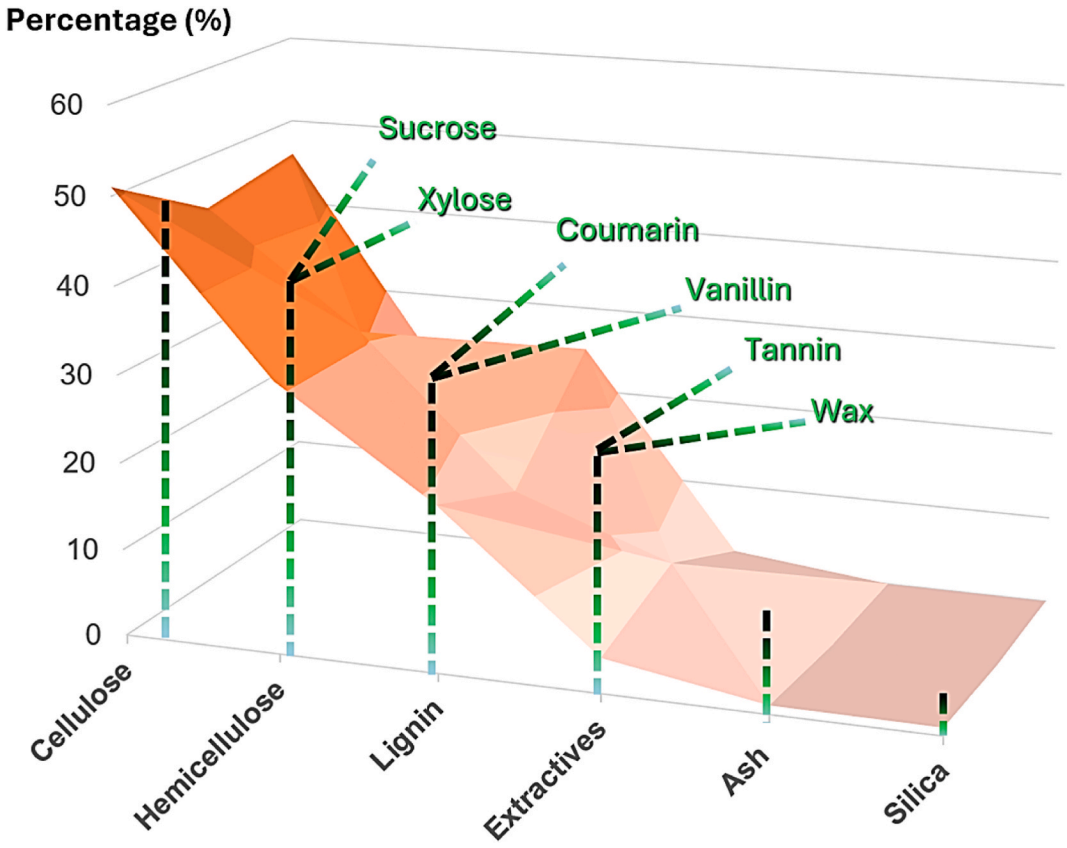

Fig. 1. Commodity load in the oil palm fruit bunch vascular bundles hailed in the market as the "dried long fibre" based on scholarly sources [9–16].

production. Prior works on transforming EFB to NFC [11–15,31] unveiled three essential processing stages: fibre extraction, purification and intensive diminution. EFB as feedstock in fibre extraction with subsequent lignin removal steps and diminution of fibres are the critical processes leading to the desired NFC. Ferrer and team [11] materialised the like of NFC from EFB by the multistage

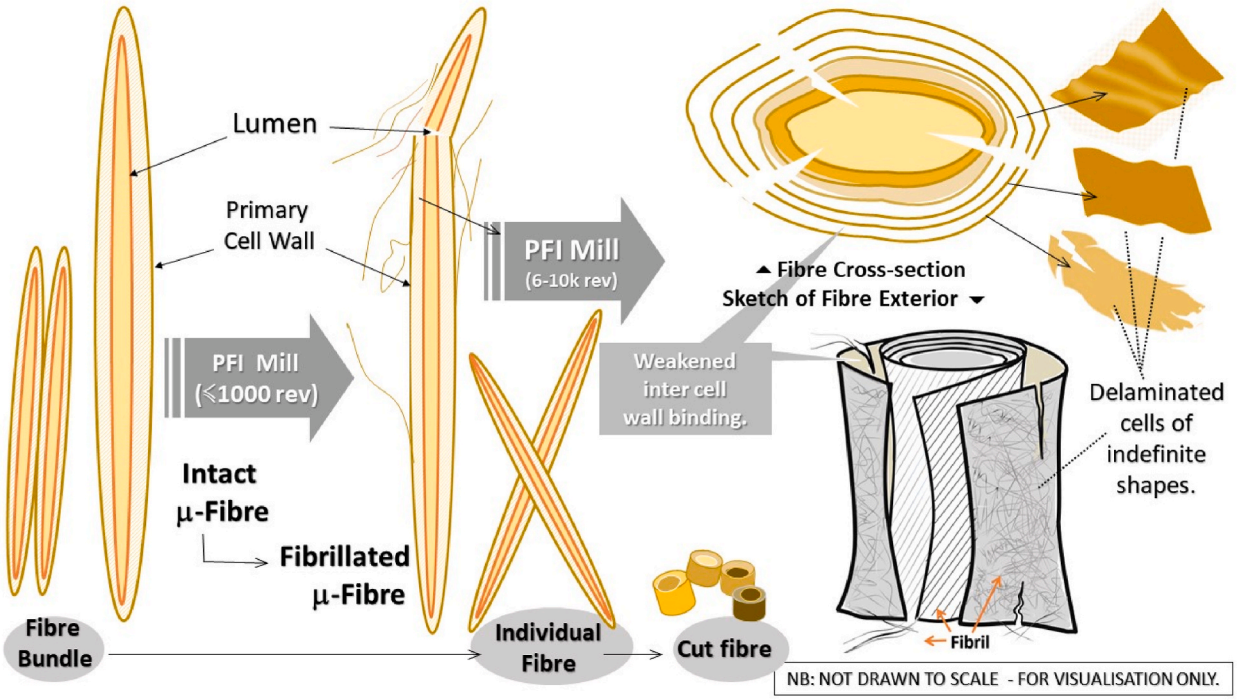

(a)

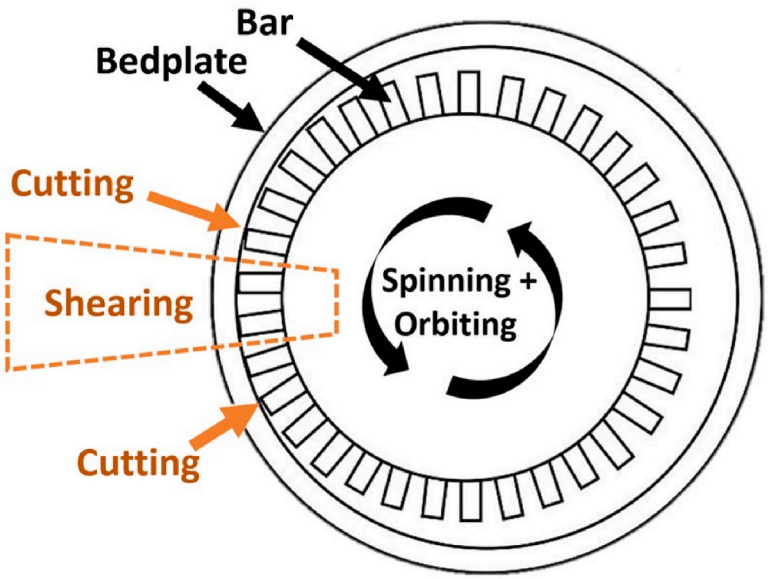

(b)

Fig. 2. DIOR-PFI synergistic impacts (a) at two principal energy phases versus the mixed forms of liberated cells and (b) schematic of PFI mill showing the bar spin direction, bedplate and the friction regions exerting shearing and cutting effects.

mechanical milling of unbleached fibres derived from the soda-anthraquinone (soda-AQ) technique. Nanometre cellulose was obtainable by refining, ultra-high energy milling, followed by microfluidisation for diminuting the solvent-cleansed fibres. Fareezal and co-workers [13] used soda-AQ pulp as a precursor and removed the non-cellulosic components to the maximum by seven-stage bleaching to yield cellulose I. The nano-fibrillated cellulose emerged upon ultrasonication. Similar steps were adopted by Fatah and team [12], where the soda-AQ technique was employed to extract EFB fibre followed by cold alkaline peroxide bleaching, acid hydrolysis, centrifugation and high-speed homogenisation [12]. Decided by the fibre extraction technique, the NFC yield was approximately 30% based on the yield of the soda-AQ pulping technique. From the economic perspective, the enormous capital entailing the complex, low-yield and time-consuming process imposes a magnificent risk. With the track record of EFB-fed pulping mills ceasing pulp production [32–34], the practicality of adopting EFB is discredited mainly due to the scattered biomass sources. Such issues are resolvable by availing a standardised process that flexibly operates on-site on a small to micro scale, reducing the capital-related risks by a narrowed materials and energy loop.

1.3. Resource-efficient process and product alternatives

This study adapted the alkaline peroxide lignin modification concept to the oil palm empty fruit bunch, EFB. We maximised the dioxydanyl radicals (DIOR) generated upon premixing hydrogen peroxide with sodium hydroxide at high alkalinity (Reaction 1).

$$H_2O_2 + OH^- \rightarrow \underset{\text{Dioxydanyl radicals(DIOR)}}{\cdot OOH} + H_2O \quad (1)$$

These radicals-initiated electron localisation and cleavage of the aromatic ring into an aliphatic moiety, denoted ‘radical-altered lignin’ or “RADIAL”. The resultant ‘dearomatisation’ is outlined in Reaction 2.

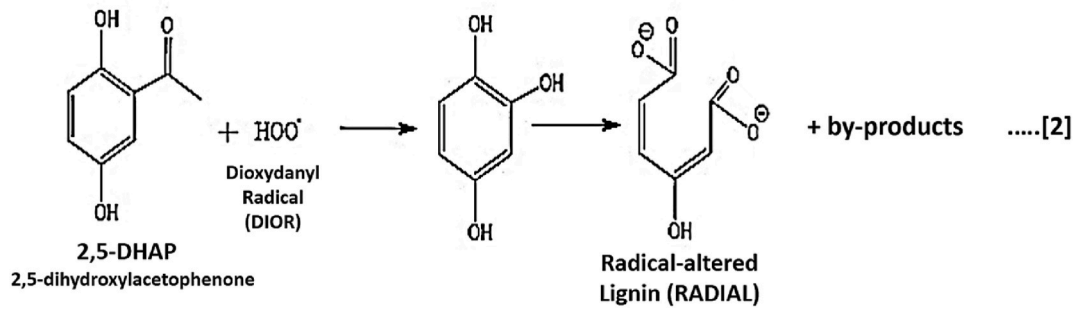

Dioxydanyl radicals (DIOR) engendering lignin conversion to auxochromic molecules [9,35–39] was the driver for the two-in-one cellulose extraction and photo-stabilizing processes, which delineated the method to other fibre extraction techniques. Going independent of pressurised digester and eliminating the need for a separate bleach plant is the instantaneous path to capital-saving [35,36]. The lignin modification concept driven by DIOR allows the system to offer high-yield and high-brightness output, fulfilling the resource efficiency criteria posited by Pena et al. [40]. Thus, nano cells comprising cellulose and non-cellulose from the EFB-DIOR-Diminution retain >95% yield profile. Being a mandatory feature of circularity, resource-efficient criteria warrant the technique’s flexible adaptation to the small and medium enterprises (SMEs), which are currently the backbone contributors to the gross domestic product (GDP) of numerous global nations [41]. The inclusivity of SMEs in emerging economies [42] is critical for the smooth transition to a circular bioeconomy.

This study extends the innovative fibre extraction principles developed by Cort and Bohn [35] to the circular management of EFB incorporating nanotechnology with Reaction 2 as the theoretical basis for biomass structural perturbation (Fig. 2a). Subjecting the feedstock containing significant RADIALS with such mechanical impact as the applied PFI milling (Fig. 2b) caused the fibre cell wall to collapse. Fig. 2a schematises the deconstruction effects and the underlying impacts based on the examined tensile profile versus the cell morphological transition [42].

At half the maximum PFI milling ever reported for EFB [11], the fibre web’s resistance to the pulling forces revealed an extraordinary tensile index (54 mN/g [42] arising from the synergy between sophisticated molecular scale bonding amongst the heterogenous cell mass (Fig. 2a). The mechanical interlocking, interdiffusion, electrostatic, capillary bridge, micro-compression, hydrogen bonding, van der Waals forces as well as the C–O::H related hydrogen bonding [43,44] were plausibly the influential binding forces amongst the generated cells. As a result, the resistance to pulling bolstered, ruling out the tensile-impeding effects of the cut and shortened fibres in Fig. 2a.

Indeed, earlier research on alkaline peroxide pulping of EFB proved the possibility of a high-strength fibre web that was only imperfect for recycling. The drawback is grievous considering the existing 680,000 trees-equivalent local paper wastes [45] and those occupying 10–40% of worldwide landfills. Thus, attempts to divert such non-recyclable fibres [39,46] and transform them into a value-added commodity is a saviour move towards a “*closed, extended, and intensifying loops strategy*” described by Morales and team [47] for circularity. In this study, we transformed the non-recyclable fibres to a higher-value cell mass for microscopic, spectroscopic, and crystallographic analyses. The understanding deepened by correlating the data with the functional properties imparted by the cells

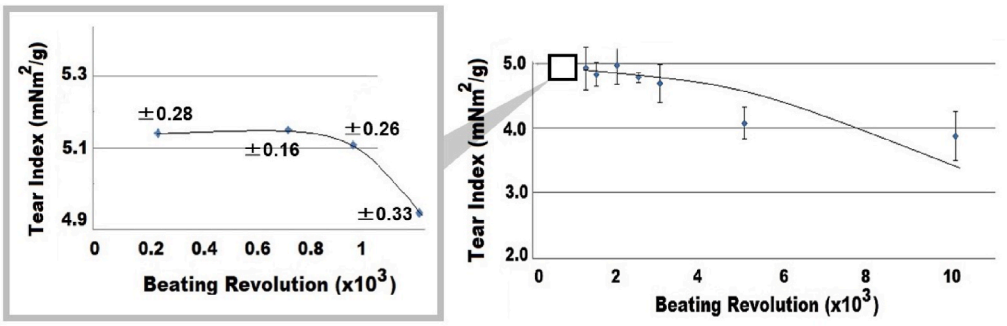

(a)

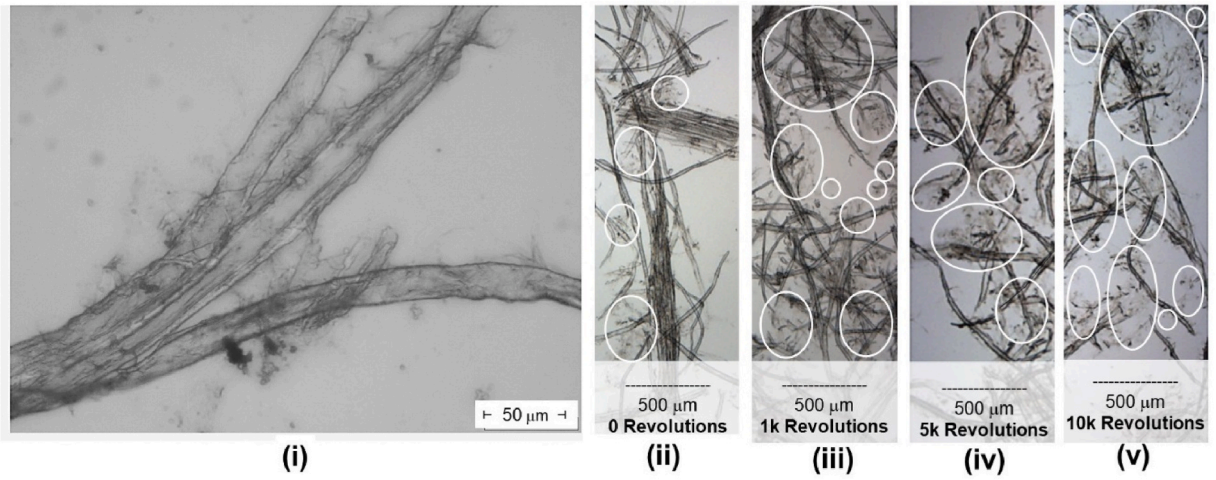

(b)

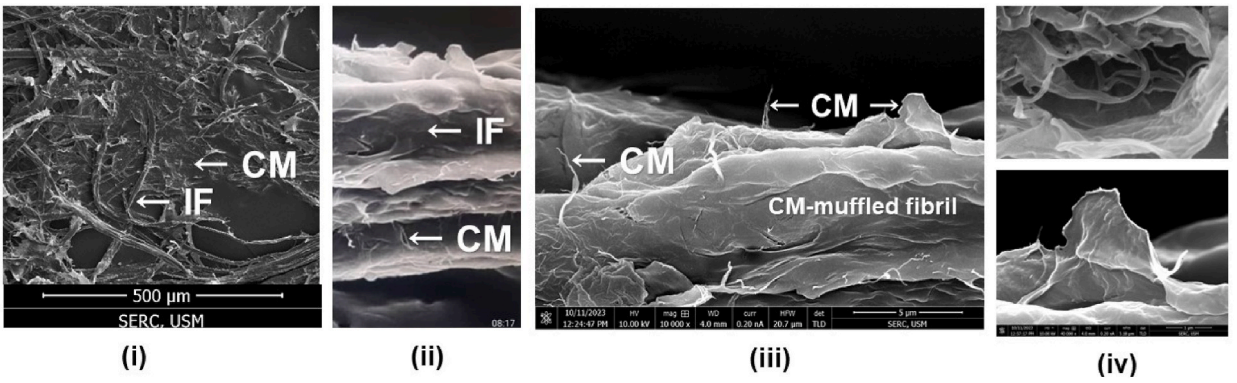

(c)

Fig. 3. Web durability versus morphological transition with beating impact portrayed on (a) the tear resistance profile, (b) the fibrous mass (i) the split end of a fibre bundle, (ii) a mix of single-fibres and fibre bundles and (iii-v) intensity of translucent cell mass (circles) correlated to (c) the non-fibril cell mass (CM) layers that form the point of defect for tearing.

in several applications. Through the findings, the process fit within the oil palm residue (OPR) circularity model was assessed.

2. Methods

The transformation of the cell with the applied mechanical energy was examined by qualitative and quantitative analyses via classical and advanced microscopy, spectroscopy and crystallography of the feedstock, the generated cells and the by-products. Mann-Whitney non-parametric significant difference assessment was run using Minitab 9.0. Related data was yield, tear indices (Fig. 3) and crystallinity derived from XRD and FTIR. The derived p-values were used to ascertain the observed trend. For replication expecting $p > 0.5$ (e.g. yield and crystallinity), the obtained percentages are reported as a range.

2.1. Morphological transition portrayed on web durability

Non-recyclable pulp from the oil palm empty fruit bunches (EFB) vascular bundles was produced by mechanical refining of the pretreated EFB. EFB (500 μm particles) pre-treatment involved reaction at 70 °C in a premixed Merck, Schubart, Germany analytical grade sodium hydroxide (4%) and hydrogen peroxide (5%) for generating perhydroxyl or dioxydanyl radical, DIOR. The temperature, ambient pressure and alkalinity were kept constant throughout the treatment duration without the use of a pulping digester. A custom design setup was employed to ensure constant contact between the biomass and the DIOR solution despite a 10-to-1 liquor-to-biomass ratio. For possessing a Kappa Number of 90% (±5%), the fibres are non-chemical pulp and acceptably a high-yield pulp or a semi-chemical pulp.

Diminution of the DIOR-treated EFB at 4% pulp consistency with Andritz Sprout-Bauer 12″ single disc refiner operating at 54.95 kWh/t specific refining energy generated micrometre fibres (micro-fibres) and fibre bundles at 85–95% yield. Intensive fibrillation via Thwing Albert Laboratory PFI milling starting from 200 to 10,000 revolutions per TAPPI T248 sp-21 (1997) [48]. Beating was performed on 4 g sample portions placed in the thoroughly cleaned PFI bedplate with the dirt-free rotating bar to achieve the calibrated impact. The total process duration was 60–90 min, depending on the applied beating revolutions and all diminution settings gave >95% yield. Webs of cells derived from each milling energy underwent tear resistance and optical tests per TAPPI (1997) Test Method T414 om-98 and T425 [49,50], respectively. Tear indices marked for each milling revolution (Fig. 3a) are the average value from ten to fifteen replicates ($10 < n < 15$). The transition from intact fibre and fibre bundles (μ-fibre web, μW) to laminae of cell walls (nano-cell web, NW) in the cell mass is taken as the predictor of "softness" in view of component redistribution and exposure tendencies. The entailing percentage change in tear web behaviour is as follows (Equation 1a and 1 b):

$$\text{Change in Tear Index (\%)} = (\text{Tear}_{NW}.\text{Tear}_{\mu W}) \,/\, \text{Tear}_{\mu W}) \times 100 \ldots \quad [1a]$$

$$\text{Difference in Tear Index (\%)} = [(\text{Tear}_{NW}.\text{Tear}_{\mu W}) \,/\, ((\text{Tear}_{NW} + \text{Tear}_{\mu W})/2)] \times 100 \ldots \quad [1b]$$

2.2. Cell microscopy

The 3D appearance of delaminated cells was captured using Leo Supra 50VP Carl Zeiss Scanning Electron Microscope (SEM). The standard R200 or 'accepts' amongst the pulp mass is denoted microfibres or "***μ***-fibre" and the PFI-milled cells registered with the "TRX-cells®" trademark are also referenced as "nano cells" and "TRX", interchangeably.

High-resolution Transmission Electron Microscopy (HRTEM, FEI TECNAI G2) of the obtained cells mounted on copper and lacey carbon grids enhanced the qualitative and semi-quantitative elemental mapping through the Oxford X-MaxN 80 mm^2 with INCA software. A prolonged electron bombardment triggering rupture of the non-conductive hydrocarbon cells was the mark for differentiating the cells from the lacey carbon.

2.3. Relative crystallinity

X-ray Diffraction (XRD), designed for clearcut crystallography of inorganic crystal lattices, was employed to benchmark the overall crystallinity transition of the feedstock to nano cells. Crystallinity values commonly derived from XRD were used to probe the raw changes of the cell mass while specific changes in the organic functional groups related to DIOR reaction with EFB were spotted in Fourier Transform Infrared (FTIR) relative crystallinity. The X-ray Diffractograms of the raw material (Biomass Feedstock), microfibre (***μ***-fibre) and the nano cells or TRX-cells® were compared. XRD was performed on a goniometer using CuKα anode radiation generated at 40 kV and 35 mA. The CuKα radiation consists of Kα1 (0.15406 nm), Kα2 (0.15443 nm) and the subtracted Kβ2 (0.13923 nm) component. The 0.5–1 mm slits were fixed for a 320 mm goniometer working radius to handle signals from approximately 0.5–1 g dried samples mounted onto a quartz stub. Samples' crystallinity indices (CI) were calculated from the height ratio between the intensity of the crystalline peak ($I_{200} - I_{AM}$) and total intensity (I_{200}) after correction for the background signal (Equation (2)). The crystallinity index was derived from equation (2), deemed the most robust measure for crystallinity derivation proposed by Park and team (2010) [51].

$$\text{Crystallinity Index, CI} = (I_{200} - I_{AM}) / (I_{200}) \ldots\ldots \quad [2]$$

Fourier Transform Infrared (FTIR) spectra of the soft matter possessing weaker intercomponent bonds (cf. inorganic crystal latices) typical of cellulosic samples (EFB feedstock, dioxydanyl-reacted refined EFB ('μ-fibres') and PFI-milled mass) were acquired using the PerkinElmer's Frontier FT-IR/NIR interfaced with MIR-TGS detector and UATR accessories. A total of 16 cumulative scans were taken, at a resolution of 8 cm^{-1}, in the default frequency range of 4000-650 cm^{-1}. Similar to the work of Ciolacu and team [52], crystallinity values were then derived from the ratio of the absorbance signals (Abs) corresponding to bands sensitive to crystallinity changes at 2900 cm^{-1} with the relatively unsusceptible band at 1372 cm^{-1} as indicated in Equation (3).

$$\text{Crystallinity} = Abs_{2900}/Abs_{1372} \times 100 \ldots. \ldots. \ldots \quad [3]$$

2.4. Spectroscopic analysis

Functional group transformation was also tracked via PerkinElmer's Frontier FT-IR/NIR interfaced with the MIR-TGS detector and UATR accessories. The nano cell isolates were dried and analysed in triplicate. Dearomatisation, referencing the cleavage of the benzene ring due to electron localisation in the presence of dioxydanyl radical, was detected by examining the 1000-1500 cm^{-1} region.

Peroxide consumption, tracking dioxydanyl-radical reaction with lignin, was determined by detecting the colour of the peroxo-molybdic acid complex (PMAC) via Shimadzu UV-Visible 1601 PC Spectrophotometer. PMAC's yellow colour formed from 2.4 molybdate binding to peroxide to form the peroxo-molybdic acid complex. 2.4 molybdate was prepared by dissolving 0.10 g of $(NH_4)_6Mo_7O_{24}.4H_2O$ in 250 ml 0.5 M sulfuric acid. Calibration standards containing 2, 4, 8, 12, 16, and 20 μl hydrogen peroxide solution (30%) in 5 ml of the molybdate solution were prepared using distilled water. In duplicate, 500 μl spent liquor was added to 5 ml 2.4 molybdate agent and homogenised by manual shaking before filtration.

2.5. Saccharide speciation

Analysis of sugar monomers was performed in accordance with the standard method in TAPPI T249 [53]. Hewlett Packard HP 6890 Gas Chromatograph interfaced with Supelco SP-2380 Fused Silica capillary column operating at 13 psi pressure with 20 cm/s gas flow and a 100 split-ratio performed the speciation. The set oven temperature was 250 °C and the injection temperature was 275 °C.

2.6. Circularity fit assessment

Tagging the waste-derived commodity to the commercialised and experimented products [10,16–18,46,54–56] into the pre-described basic circularity model [57] allowed the extension of the waste transformation routes. Ample considerations on industrial symbiosis and the criteria for organic and inorganic carbon sequestration described in the literature [58,59] set the predictor for carbon fixation at the midpoint. The parameters and the details on the relevant works exemplifying the residues fit into the model are simplified and presented (Table S5, Supplementary Materials) as the basis for the quantitative fit assessment.

3. Results

3.1. Cell wall delamination: transition to soft materials

The high-yield (85–95%) dioxydanyl radical-treated (DIOR-treated) EFB non-recyclable fibres witnessed a morphological transition with the resultant web durability providing a cue for the web and individual cell strengths. In contrast to the web's resistance to pulling, tear obstruction (Fig. 3a) manifested as the split fibres (Fig. 3bi) underwent an intensified PFI milling.

Evident from the tear profile (Fig. 3a), as the exposed EFB components (circles, Fig. 3b iii-v) increased, the ease of the crack to propagate in the direction of Elmendorf tearing force increased, mimicking the behaviour for soft matter [60], or mouldable materials inclusive of polymers and gels [61]. The existence of a 'process zone' [62] at the crack initiation microregion is one of the factors for materials' tear resistance, which Morries [63] attributed to the sum of the impeded tear strength of the individual constituents. Specific to the studied cells constituting the web, the decrement correlates with the degree of binding materials exposure. While the first down-trend phase is associated with the perturbation of binder (Reaction 2) that causes the fibre bundles to split (Fig. 3bi-ii), the more vivid phase of tear obstruction correlates with the extent of fibrous mass redistribution shown as the circled cell mass (CM) in Fig. 3b iii-v, which possesses lower strength than their intact fibrils (IF).

Tear, which occurs by propagation of cracks from the strain-concentrate initiation point, involves obstruction along the sacrificial bond [62]. In the case of the generated cells, the tearing occurred at the CM-IF interface (Fig. 3c), suggesting a weakening of the web as the thin cells formed the fixation points on the intact fibril in the cell web. As beating intensified, the redistributed mass of binding materials consisting of both the DIOR-reacted or the dearomatised ligno-fragment and the DIOR-resistant non-cellulosic became the interlayer binder in between fibrils. The CM-IF resulted in webs of declining tear indices similar to the profile uncovered portrayed by softwood fibres [64]. As the cell mass compacted into a 60-gsm web (Supplementary Materials, page 2), the inter-fibre micropores were filled up with the soft elements, restricting constituent mobility or ability to slide, which Eltahan [65] identified as a factor for the declining tear strength.

Facile by reaction 2, shearing at the radical-weakened cell wall binder (as the fibrous mass was sandwiched between the rotating

bar, A in Fig. 2b, and the bedplate, B in Fig. 2b) gave rise to the mass of extremely thin cells. Shearing at the lamellar binder (inter-fibre cell wall, Fig. 3b-i) was super likely compared to the cleavage of primary bonds, given the mechanical nature of the impact. Researchers [66–68] identified the DIOR-resistant hemicellulose [69], pectin, polyphenolic material, structural glycoproteins, and small quantities of proteins as constituents of the fibres' amorphous matrices. The transition to soft materials was vivid as the dried 60-gsm web formed a translucent network with 74% opacity (Supplementary document). A suspension of these cells appeared as 'clouds of matter' (Fig. 4a(i-ii)) under the light microscope and was apparent as peeled cells under the electron lenses (Fig. 4a(iii)). Judging from the tear profile, cells' softness, therefore, has inerrably increased by 26%.

Besides cell thinning (that favoured web tensile over tear resistance), segmentation of the recalcitrant lignified S2 and S3 structures upon contact with the sharp-edged bar-fibre-bedplate region (C, Fig. 2b) is evident in Fig. 4b. The image represents the heavily glued multi-layered structures [70–72] typical of monocots [73], which thickened throughout the microfibre biosynthesis [74,75,76]. The continued centrifugal forces during PFI milling smoothened a portion of the fibre film against the bedplate while a portion settled between the bars. As the microfibres peeled to thin cells, part of the cell walls liberated while the recalcitrant remained semi-detached to the parent fibres (Fig. 4a(iii) & 4 b) if not cut by the sharp PFI mill bar edges (C, Fig. 2b).

Overall, impacts from the rotor bars caused excessive fibrillation, intra-fibre bond breaking, fibre cutting (segmentation) and external fibrillation, which led to cell wall peeling or 'delamination'. Significant cellulosic and non-cellulosic redistribution, in turn, exposed the amorphous regions. In essence, the outcome of the Class 2 refining [77] was an amorphous, hydrophilic mass verified by the vibrational spectra and the x-ray diffractogram (XRD) in Fig. 5a and b, respectively.

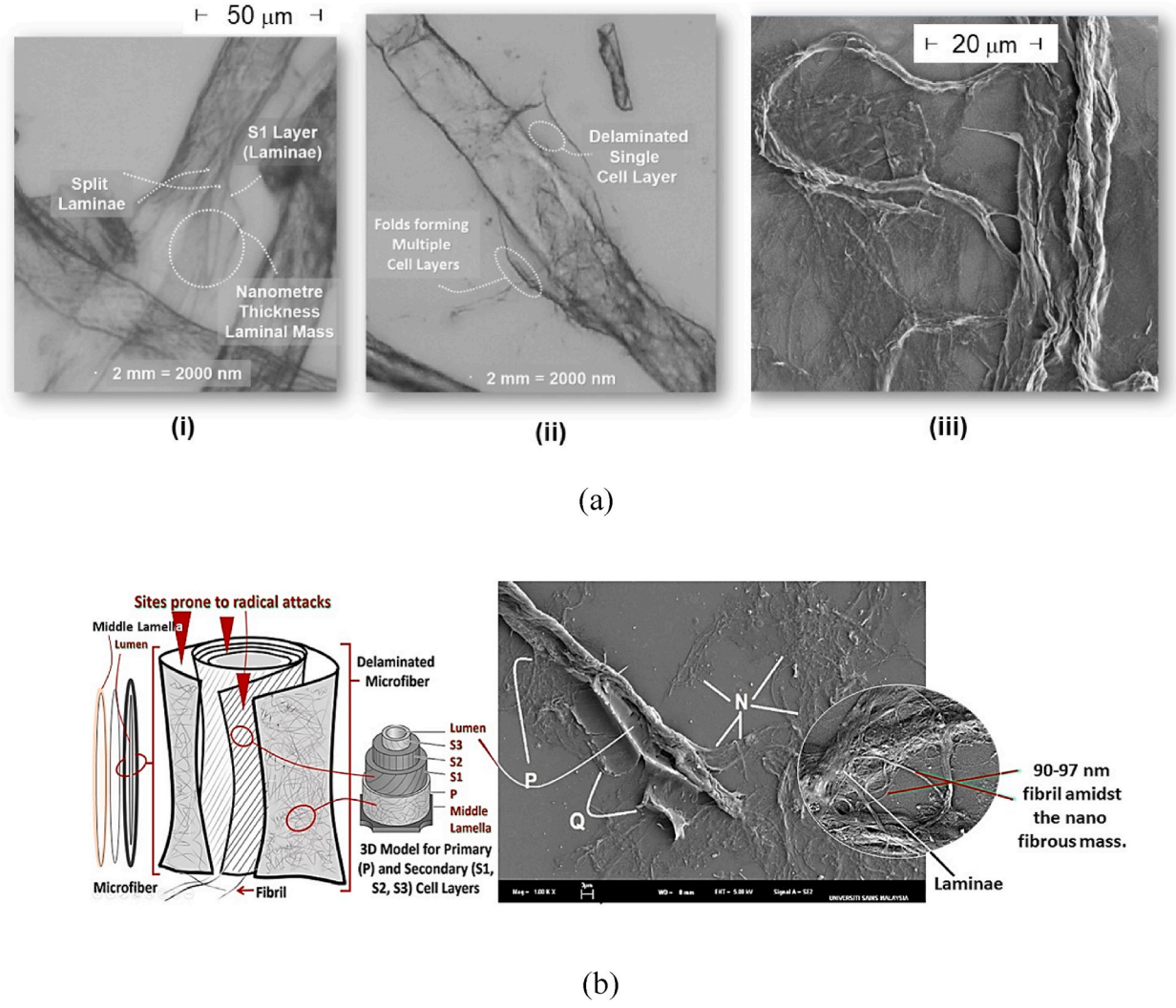

Fig. 4. Evidence of cell wall delamination showing (a) overlapping of translucent fibre with the delaminated parent fibre (i), laminae with semi-transparent cf. darker tones marking multiple cell layers (ii) and the related electron microscopic image (iii) with (b) extended evidence of cracking or vertical trim of the fibre (right) mapped to a schematic model of the fibre structure (left).

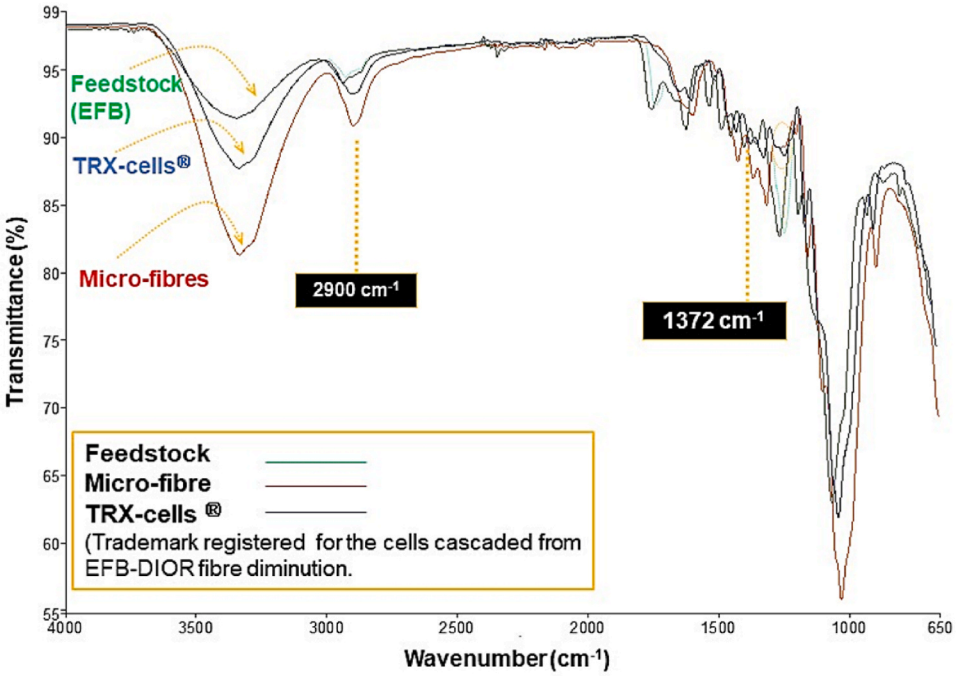

(a)

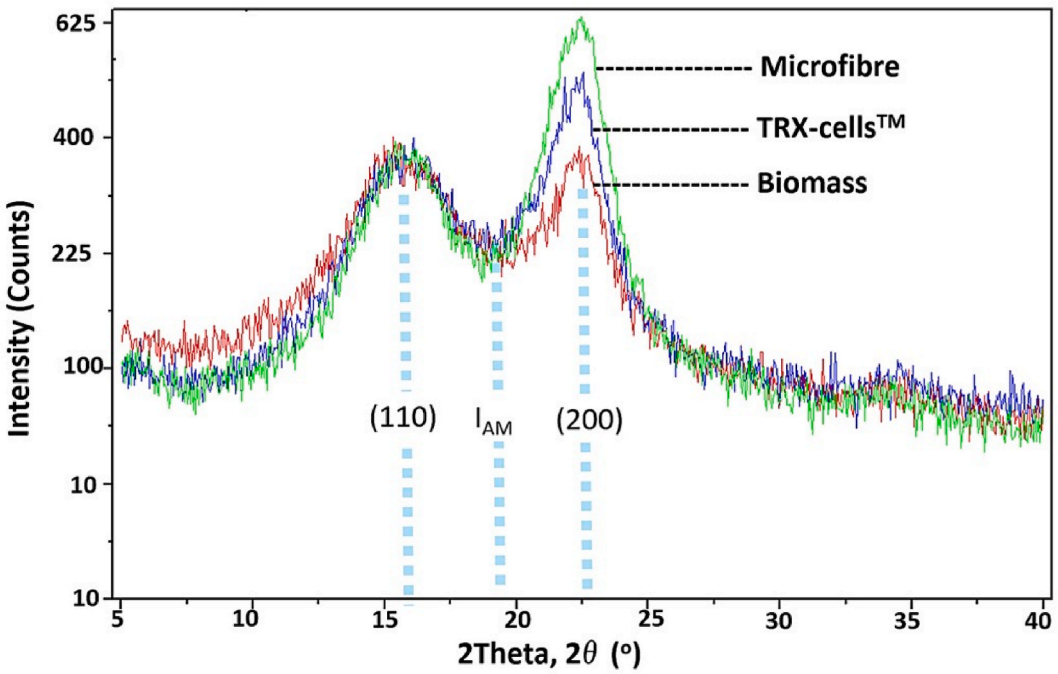

(b)

Fig. 5. FTIR and XRD analyses for approximating the relative crystallinity.

3.2. Crystallinity and dimensional accounts of softening transition

The refining stage that generated pulp mass denoted "μ-fibre" offered cell mass possessing the highest semi-crystallinity attributable to the ordered cellulose and the ordered dearomatised components surrounding the predominantly intact fibres. Extended milling, however, unravelled the radical-altered structures (RADIALS) and DIOR-resistant hemicelluloses, causing a 7–14% drop in crystallinity. Signals associated with the preferred (110) and (200) crystal lattices [78,76] show crystallinity reduction of the milled nano-scale cells (denoted TRX-cells®) attributable to the attenuated intra- and intermolecular hydrogen bond of the lignocellulosic composite. The apparent enlargement in the FTIR signal (3350 cm^{-1}) in Fig. 5a is consistent with the collective increase in the hydroxyl groups with RADIAL (Reaction 2).

Masking of the cellulosic structure, evident in Fig. 3c, arose from the redistributed hemicellulose holding the fibrils. Speciation of monosaccharide revealed 27% xylan, which is only second after glucose. The found xylan predominance (Fig. 6) is consistent with previous illumination by Rathamat et al. [79] and Thomas et al. [80], implying the supinity of xylan towards DIOR. The redistributed recalcitrant and chemically modified cells, including the non-cellulosic mass, led to an overall 31–38% crystallinity enhancement as the EFB (37–46% crystallinity) transformed to its nanoscale cell mass with 55–62% crystallinity, which is comparable to the pure cellulose nanofibers from chemical pulp [81–83]. Details of the transition are presented in Supplementary Materials, Table S3.

Tracked by the presence of the nanometre scale calcium (amongst other nano-elements, Fig. 7) via High-resolution Transmission Electron Microscopic (HRTEM) elemental mapping was the liberated middle lamella (ML) glueing the fibre bundles – an added factor to the lowered crystallinity. The detected nano calcium is plausibly associated with the calcium pectinate's role in mediating ionic interactions linking ML pectins to the pectins in the primary cell walls. The evidence also provides a matching account for cell thinning in line with ML's reported 50 nm thickness [85].

In addition, the high-resolution HRTEM testified the cell's thickness ranging from 5 to 100 nm (Fig. 8a-d), verifying the plausible presence of ML and '*fibrils embedded in hemicellulose*' [85]. As much as ML prevented living cells from sliding away from each other, it somewhat restrained the complete liberation of the fibril, defying the generated cell mass as nanorods.

In essence, alongside the cascaded TRX-cells are extractable by-products (Fig. 9a) inclusive of the nanometre scale bio-binder that co-exists with bio-inorganics. Disruption of DIOR access limits is the way towards an ultra-high yield technology (A, Fig. 9a) for nanocell production.

4. Discussion

4.1. Disrupting DIOR access limit for an ultra-high-yield bio-nanotechnology

The obtained nanoscale elements and the recalcitrant structures defined the dioxydanyl radicals (DIOR) access limits. System heterogeneity, DIOR-resistant non-lignin components and the disrupted lignified cell walls require softening actions to unlock the 100% nano cell yield.

Based on the radicals' affinity towards the high electron density molecule, the DIOR-lignin reaction led to lignin fragmentation with the radical-altered lignin (RADIAL) retained in the nano cell mass while freeing the fluorescing coumarin. The observation somewhat correlates with the illumination by Zwichmayr and co-researchers [86] despite conceptualising Reaction 2 from the light of a homogenous action of excess dioxydanyl radical towards the rate-limiting trace 2,5-DHAP in a chemical pulp. In the heterogeneous system involving EFB (possessing vanillic acid, ferulic acid and syringic acid as components of its lignin moieties [87] and coumaric acid), the extent of competing reactions is more complex as these acids are themselves free radical scavengers. The complete DIOR consumption (Supplementary Materials, Fig. S3), hints at the need to apply DIOR in strategic phases. The phases also aim to extensively reach the captured heavily lignified 'parent fibres', domiciling the amorphous constituents, which Ciolacu and team [52] identified as

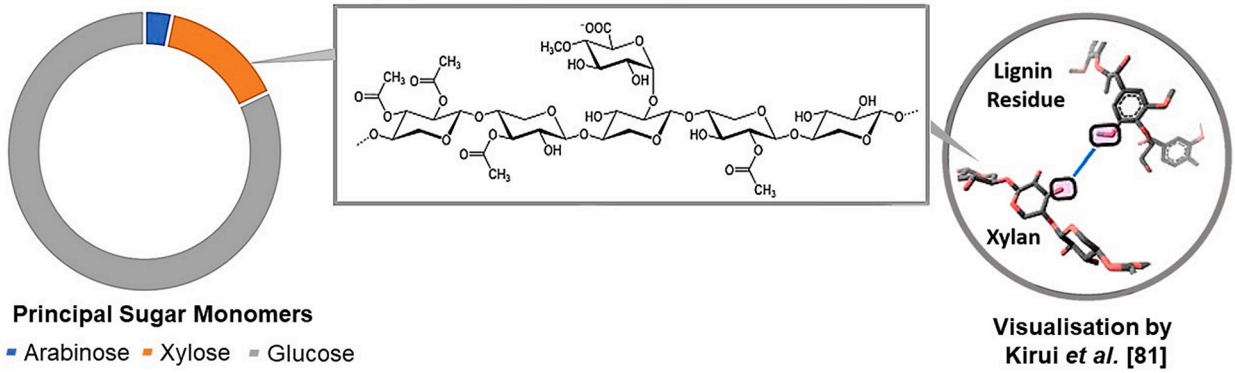

Fig. 6. Relative abundance of xylan abundance per Gas Chromatography (circle, left) and its chemical structure (square, middle) reinforcing the 3-fold xylan linkage (circle, right) to the DIOR-inaccessible hydrophobic lignin region in monocots plausibly envisioned for EFB and the unravelled cell mass. Three-fold xylan linkage reproduced under Creative Commons Attribution 4.0 International License [84].

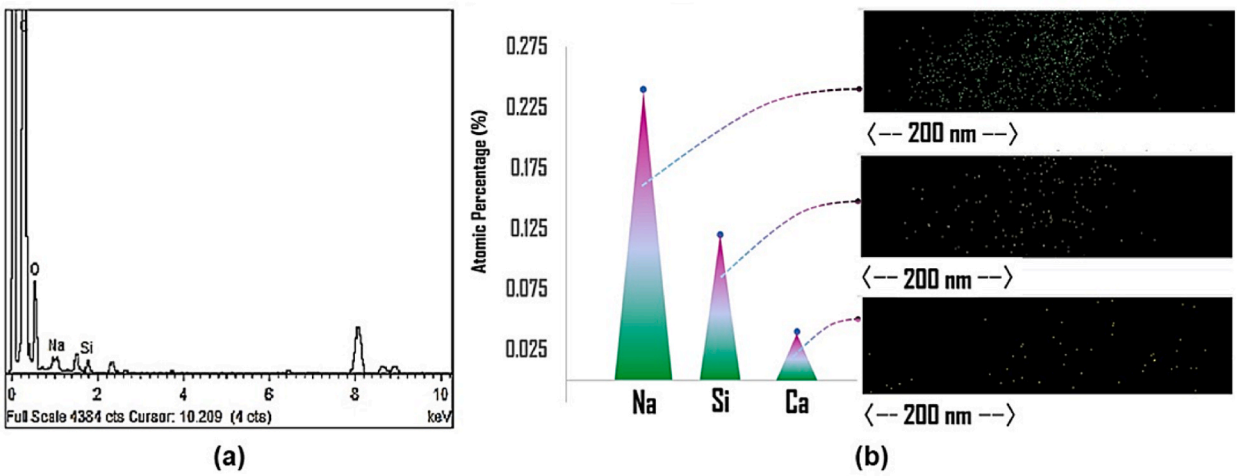

Fig. 7. Elemental mapping of nano cells showing (a) EDAX chart and (b) distribution of silicon, sodium and calcium in order of abundance in original (left) and photo-diffused (right) images with example circle marks for easy visualisation.

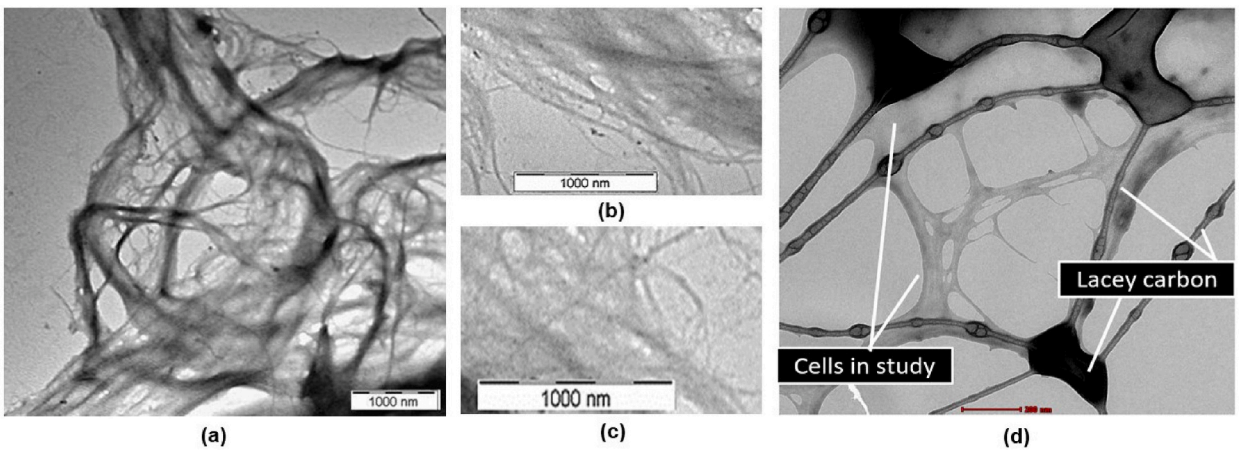

Fig. 8. Transmission-electron micrographs of nano cells revealing (a) the varying extent of fibrillation manifested as varying halftones, (b and c) a close-up look at the cell edges and (d) bright-field HRTEM of the cells rupturing upon prolonged 15 keV electron bombardment.

more prone to chemical penetration. Proper fine-tuning targeting the scissions for DIOR infusion could engender further peeling and yield of nano laminae. Further liberation of cellulose fibrils is also predictable, which in turn, leads to an intensified inter-fibril bonding, overruling the weak point obstructing the tear resistance of the cell web.

Due to the inertness of cellulose to DIOR, the strongly bound cellulose-twist [43] may define the ultimate limit to TRX yield, hence a 'vicinity to 100% yield'. Multiple cell layers co-existing as broader diameter (100 nm–200 nm) elements may include the fibrillated cellulose twist emerging as the incompletely delaminated elements. The partial delamination is apparent in the darker halftones in the isolated mass of N in Fig. 7a. Besides the non-uniformity, the nanometre diameter cellulose (Fig. 4b) and the redistributed non-cellulosic, exemplifying the mass encountered by Pinto [88], were RADIALS and sugar (Fig. 3c) constituting the middle lamella with nanometre dimension in the z-direction of the Cartesian axis, thus, fulfilling the ISO criteria for nano-objects [89].

At the crux, the generated nano cells were peels unwinding from the microfibre of EFB by 17 kWh/mt shearing impact limited by the extent of DIOR penetration. The limit of chemical consumption and delamination, in reiteration, defines the strategy for infusing DIOR and hints at the (need for) a clear-sighted move for an absolute yield of the nano-cells from EFB pulp. The more DIOR could penetrate, the higher the probability of 100% nano-cell yield, hence directing to circularity practices.

4.2. Circularity off-shooting from TRX tested applications

The amorphous cells registered as TRX-cells® pose unique interactions with other materials, offering a re-engineered surface. The saccharide-rich structural affinity for the hydrophilic and less hydrophobic regions of cellulose as Simmons et al. [70,71] and Grantham et al. [72] illuminated, led to an extensive 'web' appearance rather than individual short pure cellulose. Besides fibrils in the web

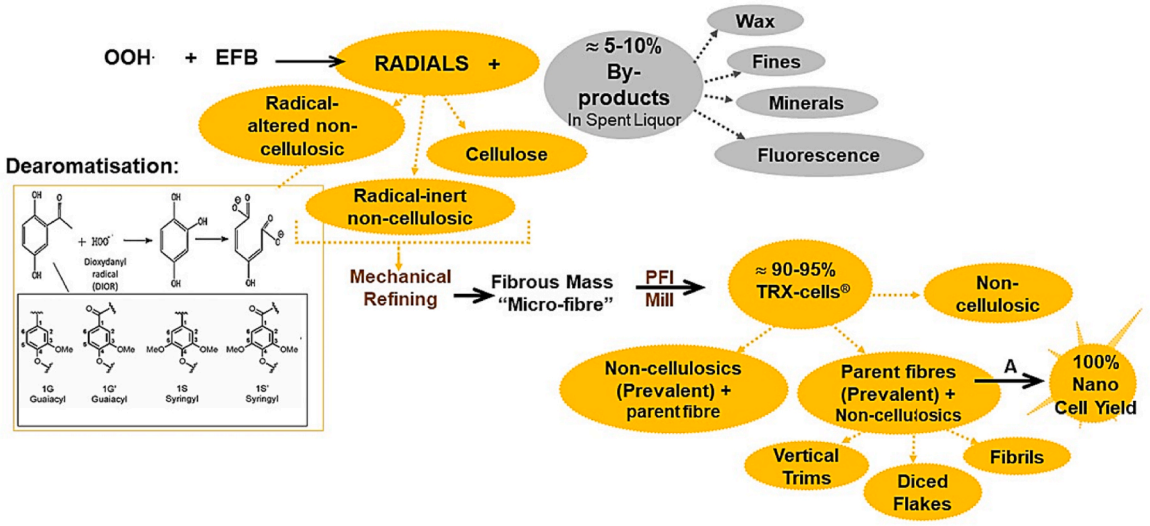

(a)

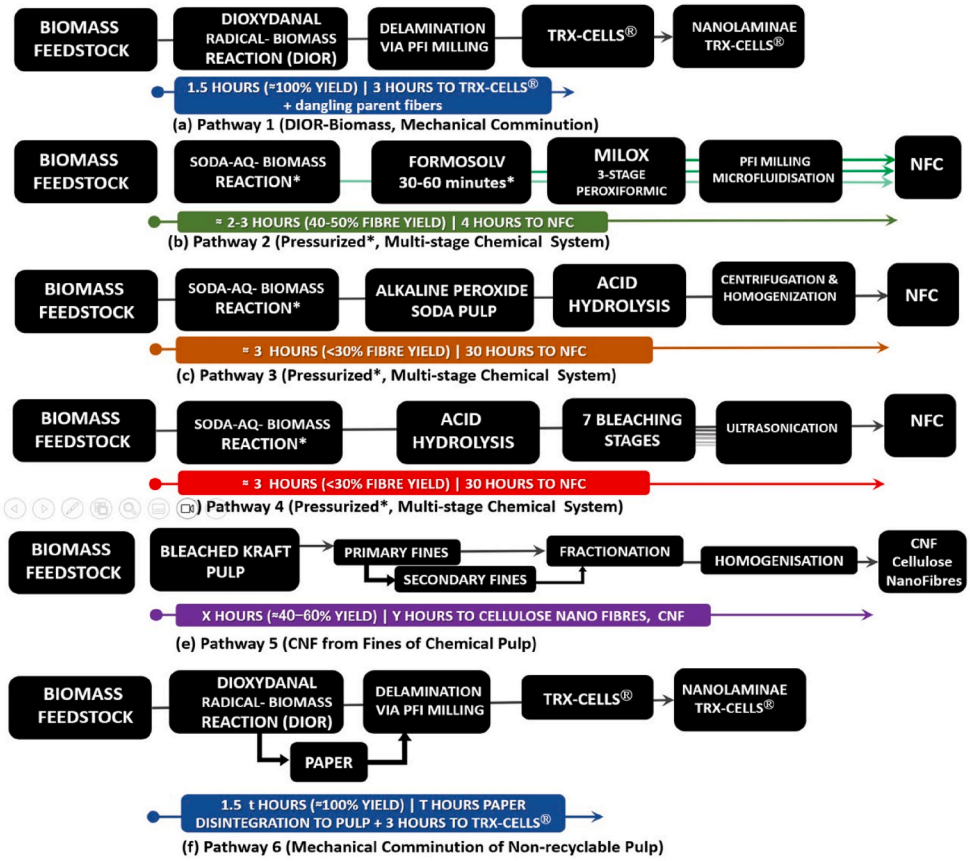

(b)

Fig. 9. Plant-derived nano fibrous mass (a) generated from a high-yield DIOR process and (b) other comparative pathways demonstrating the relative processing duration.

of sugar and RADIALS, the detected nanometre scale silicon exposure (Fig. 7) also enhanced the interaction of the cells with other surfaces via a sophisticated chemistry of nanoscale materials.

Incorporating the obtained nano cells (TRX-cells® or TRX) in fibre suspension in paper-making improved printability by 84% [90] while applying 0.0004% (w/v) nano cells as an external coat improved the inkjet printability of commercial 80 gsm paper by 80%. The cells' unique nature offered precision inkjet printability by several distinctive mechanisms like paper pore-masking and bridging of inter-fibre gaps. On a commercial paper web consisting of fibres and calcium carbonates, the obtained cells re-engineered the surface via an additional partial masking mechanism as TRX canopy formed atop the inorganic substance [46]. The observed canopy effects point to the cells' potential for reducing consumers' exposure to the trending nanoparticle inorganic fillers used in food packaging. TRX is, therefore, potentially a choice or substitute for the nanoparticles to avoid the debated [91–94] health threats. Further research is recommended to testify to the potential.

Besides the paper counterpart, TRX also adds functionality to critical resources. As rice grain coatings, the cells provided superb pigment immobilisation dendrites. Coupled with the observed thermo-blanketing, the overall effect was the functional grain longevity, extending the shelf life to more than a year without moulding [56]. Recent discovery on the preservative tribute imparted by co-heating xylan [95] rationalises the observed grain longevity. The function is an addition of simpler preservation nanotechnology to the existing food preservation technology, potentially useful as a food security measure. Against all odds, an extended study reveals that a specific cell size enhanced the flexural strength of gypsum waste that would otherwise heap at the dump site. The illumination closes the construction resource management loop, joining other forces [96] to establish circularity in construction waste management. Indeed, gypsum-TRX integration also marks the "double industrial symbiosis", considering both entities are of waste origin.

Resource efficiency achieved by time economy and zero-waste via by-product handy usability are mandatory circularity features. The major attributions lie in the absence of cellulose purification steps, rapid refining for microfibre liberation and the 20-min maximum duration for PFI milling, resulting in 83–90% shorter time (Fig. 9b) to yield the nano-functional materials. The lignin modification concept replacing delignification minimises leaching residue, simultaneously engendering an ultra-high-yield DIOR process. The feature gives rise to simple resource recovery from the spent liquor ("Resource Recovery", Fig. 10), one of which is process water recovery by membrane isolation of wax and fluorescence for automotive glazing. All combined, the DIOR process stages crucial sustainability features to enhance the nano-cells' chances for commercial exploitation. Optimal use of specific EFB particle size for TRX production saw the minerals-rich fines as a commodity for pollution adsorbent application [55] and channelled other sizes for applications premised on carbon sequestration.

Fig. 10 presents the snapshot of TRX-cells production ("TRX-cells® Pigment Immobiliser", Fig. 10) that places the process snugly in the circular oil palm residue management model. The circular resource management within TRX production itself is much simpler than the envisioned framework for NFC or bioethanol production from EFB in the prior analyses [45].

The model in Fig. 10 also houses the already materialised Thai mushroom production [10] using EFB as a growth substrate. The idea has unlocked EFB as a practical feedstock for bioethanol production (EFB for Biofuel, Fig. 10) post-mushroom harvest for the food and pharmaceutical markets. The bundle-income model allows Thailand to reap revenue while preparing the feedstock for a renewable energy material and simultaneously minimising waste alongside bioethanol generation. The model also envisions the oil palm industry as the quadruple-edge revenue analogous to the biomass circularity model of the rubber and rubberwood industry [57]. Actualisation of the model would enhance the GDP contribution from the palm oil milling sector through SME embossment that activates the cash flow from the primary harvest and its derivatives, as well as from the productive residue management and the pertaining derivatives. Such a loop of resource use has proven critical for many industries [97,98] to not only thrive to the test of time and global economic turbulence but also revive after a forced halt.

5. Strengths and limitations

A high-precision nanoscopic qualitative analysis allowing discrimination between xylan and other carbohydrates would aid the cell mass visualisation to further work on surface engineering for variable properties. Such a result would also help verify that the point of defect disrupting tear resistance was xylan, as implied by FESEM. The established outcome, however, has provided a clear direction for TRX-cells' applications in paper-based products demanding a pleasurable feel for tearing. Among the nano-scale cells serving the proven dual advantage of nano-enabled coating, xylan was the prominent one that broke the code for an alternative food preservation technology. On the macro scale, the rapid generation of nano-functional cells is an explicit strength, placing TRX-cells® closer to prototyping for commercialisation.

6. Conclusion

Nano-enabling cells cascaded from the diminution of fibres from the dioxydanyl radical (DIOR) ultra-high yield process rerouted the fibrous non-recyclable waste to the nanotechnology process and applications. The coexisting cellulose and non-cellulose components rationalised the fascinating features of colour and composite reinforcements demonstrated for paper, grains and gypsum functionalisation. The plethora of useable commodities generated along the nano-cell production implies the process' good fit into the circularity model, fulfilling the desired *"closed, extended, and intensifying loops strategy" for ultimate carbon sequestration as end-of-life.* The potential NFC-alternative cells generated via rapid process illuminate the nanotechnology venture nestling within the circular oil palm residue (OPR) management. Leveraging the resource-efficient criteria of the DIOR system provides crystal clear directives towards the clear-sighted circular nanotechnology in EFB utilization not only to prevent waste accumulation and the associated systemic impacts from pest infestation, fouling, and open burning but also to generate profits while preparing the material for subsequent use.

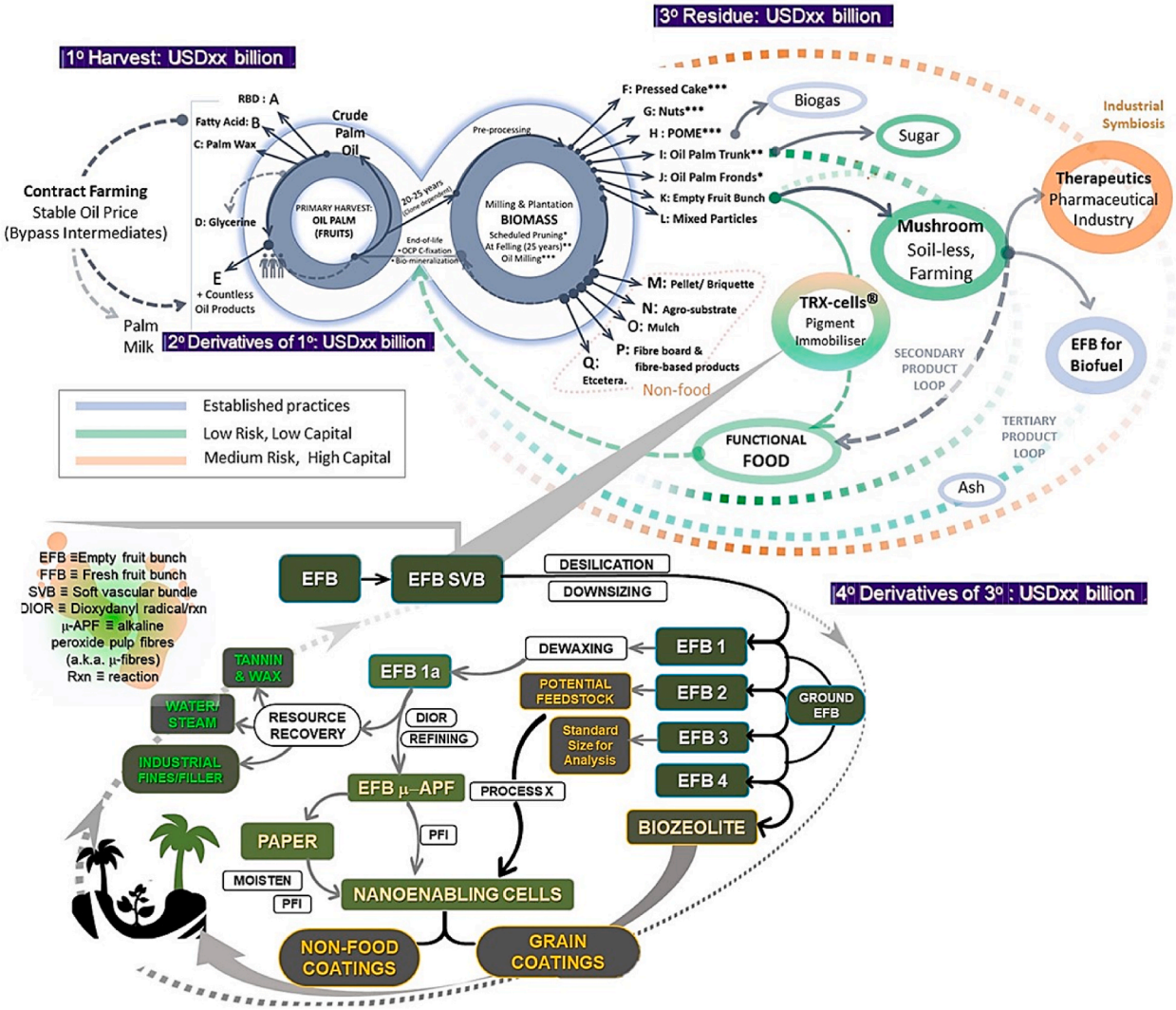

Fig. 10. EFB utilization nestling TRX production denoted "nanoenabling cells" in the overall OPR circular management model.

While reaping the prospectus commodity, the initiative fosters zero-waste and zero-emission goals commensurate with the global move toward climate change mitigation.

Data availability statement

Supplementary data will be made available upon request.

CRediT authorship contribution statement

Arniza Ghazali: Writing – original draft, Supervision, Resources, Project administration, Methodology, Investigation, Funding acquisition, Conceptualization. **Nur Haffizah Azhar:** Writing – original draft, Resources, Methodology, Investigation, Formal analysis, Data curation. **Rabeta Mohd Salleh:** Writing – review & editing, Validation. **Mohd Rafatullah:** Writing – review & editing. **Melati Khairuddean:** Writing – review & editing. **Shahrom Mahmud:** Writing – review & editing, Supervision, Resources.

Declaration of competing interest

The authors declare that they have no known competing financial interests or personal relationships that could have appeared to influence the work reported in this paper.

Acknowledgements

The authors wish to thank the Malaysia Ministry of Higher Education for funding the study through FRGS/1/2019/STG07/USM/02/8.

Appendix A. Supplementary data

Supplementary data to this article can be found online at https://doi.org/10.1016/j.heliyon.2024.e30824.

References

[1] M.L. Page, Why is there a sunflower oil shortage and what can I use instead? New Scientist. https://www.newscientist.com/article/2315466-why-is-there-a-sunflower-oil-shortage-and-what-can-i-use-instead/, 2022. (Accessed 2 December 2023).
[2] British Broadcasting Corporation, BBC, Sunflower Oil Substitutes Named by Food Watchdog, 2022. https://www.bbc.com/news/business-61271558. (Accessed 2 December 2023).
[3] Bloomberg, Palm oil resurges on Indian demand. https://www.thestar.com.my/business/business-news/2023/07/13/palm-oil-resurges-on-indian-demand, 2023.
[4] Roundtable on Sustainable Palm Oil, RSPO, From farm to plate: how sustainable is the palm oil in your food?. https://rspo.org/from-farm-to-plate-how-sustainable-is-the-palm-oil-in-your-food/, 2020. (Accessed 2 December 2023).
[5] T. Crowfoot, World Population Just Passed 8 Billion. Here Is what it Means, World Economic Forum, 2022. https://www.weforum.org/agenda/2022/11/world-population-passes-8-billion-what-you-need-to-know/. (Accessed 2 December 2023).
[6] United Nations Population Fund, UNFPA, World Population Dashboard World Population Dashboard, 2023 (unfpa.org).
[7] Grand View Research, Palm oil market size, share & trends analysis report by nature (organic & conventional), by product (RBD palm oil, palm kernel oil), by end-use (pharmaceuticals), by region, and segment forecasts. https://www.grandviewresearch.com/industry-analysis/palm-oil-market#:~:text=The%20global%20palm%20oil%20market%20size%20was%20valued,beverage%2C%20biofuel%2C%20energy%2C%20personal%20care%2C%20and%20cosmetics%20industries, 2023.
[8] V. Voora, S. Bermudez, J.J. Farrell, C. Larea, E. Buna, Palm oil production continues to grow to match increasing demand. Global Market Report. Palm Oil Prices and Sustainability, 2023.
[9] A. Ghazali, W.D. Wanrosli, K.N. Law, Alkaline peroxide mechanical pulping of oil palm lignocellulosics: Part 2-EFB responses to pretreatments, Appita J. 59 (1) (2006) 65–70.
[10] C. Mamimin, S. Chanthong, C. Leamdum, S. O-Thong, P. Prasertsan, Improvement of empty palm fruit bunches; biodegradability and biogas production by integrating the straw mushroom cultivation as a pretreatment in the solid-state anaerobic digestion, Bioresour. Technol. 319 (2021) 124227.
[11] A. Ferrer, I. Filpponen, A. Rodríguez, J. Laine, O.J. Rojas, Valorization of residual Empty Palm Fruit Bunch Fibers (EPFBF) by microfluidization: production of nanofibrillated cellulose and EPFBF nanopaper, Bioresour. Technol. 125 (2012) 249–255.
[12] I.Y.A. Fatah, H.P.S. Abdul Khalil, M.S. Hossain, A.A. Aziz, Y. Davoudpour, R. Dungani, A. Bhat, Exploration of a chemo-mechanical technique for the isolation of nanofibrillated cellulosic fiber from oil palm empty fruit bunch as a reinforcing agent in composites materials, Polymers 6 (10) (2014) 2611–2624, https://doi.org/10.3390/polym6102611.
[13] A.W. Fareezal, M.A. Izzati, M.Z. Shazana, I. Rushdan, R. Rosazley, Z.M.A. Ainun, Characterization of nanofibrillated cellulose produced from oil palm empty fruit bunch fibers (OPEFB) using ultrasound, Journal of Contemporary Issues and Thought 6 (2016) 30–37.
[14] M.N.M. Ibrahim, Vanilla from black liquor, Buletin Kimia USM 5 (2013). http://eprints.usm.my.
[15] F.N.M. Padzil, H.S. Lee, Z.M.A.A. Asaari, H.L. Ching, L.C. Abdullah, Potential of oil palm empty fruit bunch resources in nanocellulose hydrogel production for versatile applications: a review, Materials 13 (5) (2020) 1245, https://doi.org/10.3390/ma13051245.
[16] S. Chanlongphitak, S. Papong, P. Malakul, T. Mungcharoen, Life cycle assessment of palm empty fruit bunch utilization for power plants in Thailand. International Conference on Biological, Environment and Food Engineering (BEFE-2015) May 15-16, 2015. Singapore.
[17] Kingman, How to start a palm EFB briquette plant. https://www.woodbriquetteplant.com/news/Palm-EFB-Briquette-Press.html, 2021. (Accessed 25 November 2023).
[18] F.G.V. Holdings Berhad, FGV products. https://www.fgvholdings.com/wp-content/uploads/2021/02/FGV-Products-Brochure.pdf, 2021. (Accessed 25 November 2023).
[19] L.A. Job, Chlorine in the cellulose pulping industry, [Written Speech] Johannesburg (1942).
[20] T. Aziz, F. Haq, A. Farid, M. Kiran, S. Faisal, A. Ullah, N. Ullah, A. Bokhari, M. Mubashir, L.F. Chuah, P.L. Show, Challenges associated with cellulose composite material: facet engineering and prospective, Environ. Res. 223 (2023) 115429, https://doi.org/10.1016/j.envres.2023.115429.
[21] L.V. Hai, L. Zhai, H.C. Kim, J.W. Kim, E.S. Choi, J. Kim, Cellulose nanofibers isolated by TEMPO-oxidation and aqueous counter collision methods, Carbohydrate Polymers 191 (2018) 65–70, https://doi.org/10.1016/j.carbpol.2018.03.008.
[22] A. P. Martínez-Ramírez, S. A. Rincón-Ortiz, V. G. Baldovino-Medrano, C. Blanco-Tirado, M. Y. Combariza, TEMPO Oxidation for High Cellulose Content Biomass: A Study on Palm Oil Empty Fruit Bunch Fibers, Res Square, https://doi.org/10.21203/rs.3.rs-3186311/v1.
[23] A.P. Martínez-Ramírez, S.A. Rincón-Ortiz, V.G. Baldovino-Medrano, C. Blanco-Tirado, M.Y. Combariza, Influence of reaction variables on the surface chemistry of cellulose nanofibers derived from palm oil empty fruit bunches, RSC Adv. 13 (2023) 36117.
[24] E. Brannvall, C. Aulin, CNFs from softwood pulp fibers containing hemicellulose and lignin, Cellulose 29 (2022) 4961–4976, https://doi.org/10.1007/s10570-022-04585-8.
[25] A. Winter, B. Arminger, S. Veigel, et al., Nanocellulose from fractionated sulfite wood pulp, Cellulose 27 (2020) 9325–9336, https://doi.org/10.1007/s10570-020-03428-8.
[26] M.A.F. Supian, K.N.M. Amin, S.S. Jamari, S. Mohamad, Production of cellulose nanofiber (CNF) from empty fruit bunch (EFB) via mechanical method, J. Environ. Chem. Eng. 8 (1) (2020) 103024, https://doi.org/10.1016/j.jece.2019.103024.
[27] N. H. S. Jafri, D. N. Jimat, W. M. F. W. Nawawi et al., Screening of deep eutectic solvent mixtures for treating empty fruit bunches to obtain cellulose nanofiber, Mater. Today: Proc., https://doi.org/10.1016/j.matpr.2023.04.54.
[28] J. Zeng, Z. Zeng, Z. Cheng, et al., Cellulose nanofibrils manufactured by various methods with application as paper strength additives, Sci. Rep. 11 (2021) 11918, https://doi.org/10.1038/s41598-021-91420-y.
[29] K.P.Y. Shak, Y.L. Pang, S.K. Mah, Nanocellulose: recent advances and its prospects in environmental remediation, Beilstein J. Nanotechnol. 9 (2018) 2479–2498.
[30] P. Kaur, N. Sharma, M. Munagala, R. Rajkhowa, B. Aallardyce, Y. Shastri, R. Agrawal, Nanocellulose: resources, physio-chemical properties, current uses and future applications, Front. Nanotechnol. 3 (2021) 747329, https://doi.org/10.3389/fnano.2021.747329.
[31] A. Ferrer, I. Filpponen, RodrígueZ, J. Laine, L. Jiménez, O.J. Rojas, Residual palm fibers from empty fruit bunches (EFB): production of nanofibrillar cellulose films, in: 13th Congresso International en Ciencia y Technologie de Metallurgia y Materials, vol. 2013, 2013.

[32] R. Cheah, World's First Oil Palm-Based Pulp Paper. The Star, 2008. https://www.etawau.com/OilPalm/PulpPaperMill.htm. (Accessed 25 November 2023).
[33] R. Ibrahim, Research and Development (R&D) works on non-wood species by pulp and paper laboratory [Webinar]. Forest Research Institute Malaysia. 5th Wood and Biofibre International Conference, 2021.
[34] A. Ghazali, Reconceptualizing industrial by-products: biomass circularity for people and nature, in: R.T. Kapoor, Mohd Rafatullah (Eds.), Bioremediation Technologies: for Wastewater and Sustainable Circular Bioeconomy, De Gruyter, 2023, pp. 23–56, https://doi.org/10.1515/9783111016825-002.
[35] C.J. Cort, W.L. Bohn, Alkaline peroxide mechanical pulping of hardwoods, TAPPI Journal 74 (6) (1991) 79.
[36] H. Bukhart, B. Pelech, D.I.H. Munster, New BCTMP grades for quality improvement and cost reduction of paper machine furnishes. Proceedings of the 54th Annual Convention of ATIP, France, 2001, pp. 9–11.
[37] E.C. Xu, APMP pulps from non-wood fibres. Part 1: kenaf and straw, Appita J. 54 (5) (2001) 444–448.
[38] Y.M. Dermawan, A. Ghazali, W.D. Wanrosli, Effect of multiple impregnation on APP of EFB, Cellul. Chem. Technol. 45 (5–6) (2011) 355–360.
[39] N.H. Kamaluddin, A. Ghazali, W.D. Wan Rosli, Potential of fines as reinforcing fibres in APP of OP EFB, Bioresources 7 (3) (2012) 3425–3438.
[40] C. Pena, B. Civit, Gallego, A. Schmid, A. Druckman, A. Caldeira- Pires, B. Weidema, E. Mieras, F. Wang, J. Fava, l. Milà i Canals, M. Cordella, P. Arbuckle, S. Valdivia, S. Fallaha, W. Motta, Using life cycle assessment to achieve a circular economy. Life Cycle Initiative, 2020. https://pure.manchester.ac.uk/ws/files/175169708/Pena_et_al_2020_Using_LCA_to_achieve_circular_economy_LCI_July_2020.pdf.
[41] World Bank, Small Medium Enterprises (SMEs) finance - improving SMEs' access to finance and finding innovative solutions to unlock sources of capital. https://www.worldbank.org/en/topic/smefinance, 2023.
[42] A. Ghazali, M.R.H. Mohd Zukeri, W.D. Wanrosli, B. Azahari, R. Ibrahim, T. Ahmed, I. Rushdan, A.K. Ziya, Augmentation of EFB fibre web by nano-scale fibrous elements, Adv. Mater. Res. 832 (2014) 494–499.
[43] S. Paavilainen, T. Rog, I. Vattulainen, Analysis of twisting of cellulose nanofibrils in atomic molecular dynamics simulations, J. Phys. Chem. B 115 (14) (2011) 3747–3755.
[44] M. Wohlert, T. Benselfelt, L. Wagberg, I. Furo, L.A. Berglund, J. Wohlert, Cellulose and the role of hydrogen bonding: not in charge of everything, Cellulose 29 (2022) 1–23, https://doi.org/10.1007/s10570-021-04325-4.
[45] R. Yusoff, A.N. Azizul, Towards a sustainable paper consumption and printing practices. https://news.iium.edu.my/?p=162372, 2022.
[46] A. Ghazali, N.H. Azhar, S. Mahmud, M.F. Khairudin, I. Ahmad, M. Rafatullah, M.A. Zaini, Y. Yusof, Delaminated cells for nano-enabled inkjet printability, Cellul. Chem. Technol. 55 (9–10) (2021) 1071–1081.
[47] M.E. Morales, S. Lhuillery, M. Ghobakhloo, Circularity effect in the viability of bio-based industrial symbiosis: tackling extraordinary events in value chains, J. Clean. Prod. 348 (2022) 131387, https://doi.org/10.1016/j.jclepro.2022.131387.
[48] Technical Association of Pulp and Paper Industry, TAPPI, T248 sp-21 laboratory beating of pulp (PFI mill method). TAPPI Standard Test Methods, TAPPI Press, 1997.
[49] Technical Association of Pulp and Paper Industry, TAPPI, T414 Om-98 Elmendorf Tear Resistance of Paper, TAPPI Standard Test Methods, TAPPI Press, 1997.
[50] Technical Association of Pulp and Paper Industry, TAPPI, T425 Opacity, TAPPI Standard Test Methods, TAPPI Press, 1997.
[51] S. Park, J.O. Baker, M.E. Himmel, P.A. Parilla, D.K. Johnson, Cellulose crystallinity index: measurement techniques and their impact on interpreting cellulase performance, Biotechnol. Biofuels 3 (2010) 1–10.
[52] D. Ciolacu, F. Ciolacu, V. Popa, Amorphous cellulose: structure and characterization, Cellul. Chem. Technol. 45 (1–2) (2010) 13–21.
[53] Technical Association of Pulp and Paper Industry, TAPPI, T249 Carbohydrates Composition, TAPPI Standard Test Methods, TAPPI Press, 1997.
[54] T. Ahmad, M. Rafatullah, A. Ghazali, O. Sulaiman, R. Hashim, A. Ahmad, Removal of pesticides from water and wastewater by different adsorbents: a review, J. Env. Sc. Health 4 (2010) 231–271.
[55] M. Danish, T. Ahmad, R. Hashim, M.H.R.M. Zukeri, A. Ghazali, O. Sulaiman, S. Hiziroglu, Characterization and adsorption kinetic study of surfactant treated oil palm (*Elaeis guineensis*) empty fruit bunches, Desalination Water Treat. 57 (20) (2016) 9474–9487, https://doi.org/10.1080/19443994.2015.1028456.
[56] A. Ghazali, M.S. Rabeta, M.Q. Ahmad, N.H. Azhar, M.F.A. Malik, Capturing anthocyanin immobilization on rice through the ultra-high resolution electron lenses, Malaysian Journal of Microscopy 17 (2) (2021) 20–31.
[57] A. Ghazali, M. Zbiec, Rich dad and poor dad: biomass circularity sciences empathizing rubber smallholders, Journal of Advanced Research in Applied Science and Engineering Technology 29 (1) (2022) 207–222, https://doi.org/10.37934/araset.29.1.207222.
[58] T. Jamieson, E. Sager, C. Gueguen, Characterization of biochar-derived dissolved organic matter using Uv-visible absorption and excitation – emission fluorescence spectroscopies, Chemosphere 103 (2014) 197–204, https://doi.org/10.1016/j.chemospere.2013.11.066.
[59] S. Syed, V. Buddolla, B. Lian, Oxalate carbonate pathway—conversion and fixation of soil carbon—a potential scenario for sustainability, Front. Plant Sci. 11 (2020) 591297.
[60] B. Zhang, S.B. Hutchens, On the relationship between cutting and tearing in soft elastic solids, Soft Matter 17 (28) (2021) 6728–6741, https://doi.org/10.1039/D1SM00527H.
[61] Massachusette Department of Materials Science and Engineering, MIT DMSE, Soft Matter - MIT Department of Materials Science and Engineering, 2024.
[62] K. Bircher, M. Zündel, M. Pensalfini, A.E. Ehret, E. Mazza, Tear resistance of soft collagenous tissues, Nat. Commun. 10 (1) (2019) 792, https://doi.org/10.1038/s41467-019-08723-y.
[63] B.A. Morris, Plastics design library, the science and technology of flexible packaging, in: Barry A. Morris (Ed.), Strength, Stiffness, and Abuse Resistance, Elsevier, 2017, pp. 309–350, https://doi.org/10.1016/B978-0-323-24273-8.00009-5, 2017.
[64] A. Miletzky, M. Punz, H. Weber, P. Wollboldt, R. Krasser, W. Bauer, R. Schennach, Improvement of paper strength by increasing the xylan content. Advances in Pulp and Paper Research, 2013, pp. 887–906. Cambridge.
[65] E. Eltahan, Structural parameters affecting tear strength of fabrics tents, Alex. Eng. J. 57 (2018) 97–105, https://doi.org/10.1016/j.aej.2016.12.005.
[66] K.H. Caffall, D. Mohnen, The structure, function, and biosynthesis of plant cell wall pectic polysaccharides, Carbohydr. Res. 344 (14) (2009) 1879–1900, https://doi.org/10.1016/j.carres.2009.05.021.
[67] E. Reszczyriska, A. Hanaka, Lipid composition in plant membranes, Cell Biochem. Biophys. 78 (2020) 401–414, https://doi.org/10.1007/s12013-020-00947-w.
[68] M.J. Hawkesford, I. Cakmak, D. Coskun, L.J.D. Kok, H.M. Lambers, J.K. Schjoerring, P.J. White, Functions of Macronutrients, Marschner's Mineral Nutrition of Plants, Academic press, 2023, pp. 201–281.
[69] Y.N. Solier, C.N. Schnell, M.N. Cabrera, M.A. Zanuttini, M.C. Inalbon, Alkaline-peroxide extraction of xylan from sugarcane bagasse. Characteristics and film forming capacity, Ind. Crop. Prod. 145 (2020) 112056, https://doi.org/10.1016/j.indcrop.2019.112056.
[70] T.J. Simmons, M. Durand-Tardif, S.P. Brown, R. Dupree, M. Busse-Wicher, P. Dupree, An even pattern of xylan substitution is critical for interaction with cellulose in plant cell walls, Nat. Plants 3 (11) (2017) 859–865, https://doi.org/10.1038/s41477-017-0030-8.
[71] T.J. Simmons, J.C. Mortimer, O.D. Bernardinelli, A.C. Poppler, S.P. Brown, E.R. de Azevedo, R. Dupree, P. Dupree, Folding of xylan onto cellulose fibrils in plant cell walls revealed by solid-state NMR, Nat. Commun. 7 (1) (2016) 13902, https://doi.org/10.1038/ncomms13902.
[72] N.J. Grantham, J. Wurman-Rodrich, O.M. Terrett, J.J. Lyczakowski, K. Stott, D. Iuga, T.J. Simmons, M. Durand-Tardif, S.P. Brown, R. Dupree, M. Busse-Wicher, P. Dupree, An even pattern of xylan substitution is critical for interaction with cellulose in plant cell walls, Nat. Plants 3 (11) (2017) 859–865, https://doi.org/10.1038/s41477-017-0030-8.
[73] Q. Liu, L. Luo, L. Zheng, Lignins: biosynthesis and biological functions in plants, Int. J. Mol. Sci. 19 (2) (2018) 335.
[74] G. Audesirk, T. Audesirk, B.E. Byers, Biology: Life on Earth with Physiology, Pearson, 2001.
[75] N. Mokshina, T. Chernova, D. Galinousky, O. Gorshkov, T. Gorshkova, Key stages of fiber development as determinants of bast fiber yield and quality, Fibers 6 (2) (2018) 20.
[76] D. Ye, S. Rongpipi, S.N. Kiemle, W.J. Barnes, A.M. Chaves, C. Zhu, E.D. Gomez, Preferred crystallographic orientation of cellulose in plant primary cell walls, Nat. Commun. 11 (1) (2020) 4720.
[77] X. Chen, E. Kuhn, W. Wang, S. Park, K. Flanegan, O. Trass, L. Tenlep, L. Ling Tao, M. Tucker, Comparison of different mechanical refining technologies on the enzymatic digestibility of low severity acid pretreated corn stover, Bioresour. Technol. 147 (2013) 401–408, https://doi.org/10.1016/j.biortech.2013.07.109.

[78] C. Thulluri, R. Balasubramaniam, H.R. Velankar, Generation of highly amenable cellulose-Iβ via selective delignification of rice straw using a reusable cyclic ether-assisted deep eutectic solvent system, Sci. Rep. 11 (2021) 1591, https://doi.org/10.1038/s41598-020-80719-x.
[79] Z. Rathamat, W. Choorit, Y. Chisti, P. Prasertsan, Two-step isolation of hemicellulose from oil palm empty fruit bunch fibers and its use in production of xylooligosaccharide prebiotic, Ind. Crop. Prod. 160 (2021) 113124, https://doi.org/10.1016/j.indcrop.2020.113124.
[80] P. Thomas, T. Duolikun, N.P. Rumjit, S. Moosavi, C.W. Lai, M.R. Johan, Comprehensive review on nanocellulose. Recent developments, challenges and future prospects, J. Mech. Behav. Biomed. Mater. 110 (2020) 103884.
[81] A.N. Frone, D.M. Panaitescu, I. Chiulan, et al., The effect of cellulose nanofibers on the crystallinity and nanostructure of poly(lactic acid) composites, J. Mater. Sci. 51 (2016) 9771–9791, https://doi.org/10.1007/s10853-016-0212-1.
[82] K. Daicho, K. Kobayashi, S. Fujisawa, T. Saito, Recovery of the irreversible crystallinity of nanocellulose by crystallite fusion: a strategy for achieving efficient energy transfers in sustainable biopolymer skeletons, Angew.Chem. Int. Ed. 60 (2021) 24630–24636, https://doi.org/10.1002/anie.202110032.
[83] E. Kaffashsaie, H. Yousefi, T. Nishino, T. Matsumoto, M. Mashkour, M. Madhoushi, H. Kawaguchi, Direct conversion of raw wood to TEMPO-oxidized cellulose nanofibers, Carbohydrate Polymers 262 (2021) 117938, https://doi.org/10.1016/j.carbpol.2021.117938.
[84] A. Kirui, W. Zhao, F. Deligey, H. Yang, X. Kang, F. Mentink-Vigier, T. Wang, Carbohydrate-aromatic interface and molecular architecture of lignocellulose, Nat. Commun. 13 (1) (2022) 538, https://doi.org/10.1038/s41467-022-28165-3.
[85] M.S. Zamil, A. Geitmann, The middle lamella—more than a glue, Phys. Biol. 14 (1) (2017) 015004, https://doi.org/10.1088/1478-3975/aa5ba5.
[86] N.S. Zwirchmayr, U. Henniges, M. Bacher, T. Hosoya, H. Reiter, M. Spitzbart, T. Dietz, K. Eibinger, W. Kreiner, A.K. Mahler, H. Winter, T. Röder, A. Potthast, T. Elder, T. Rosenau, Degradation of the cellulosic key chromophores 2, 5- and 2, 6- dihydroxyacetophenone by hydrogen peroxide under alkaline conditions, Chromophores in cellulosics, XVII, Cellulose 25 (2018) 3815–3826.
[87] R.C. Sun, J.M. Fang, J. Tomkinson, Fractional isolation and structural characterisation of lignins from oil palm trunk and empty fruit bunch fibers, J. Wood Chem. Technol. 19 (4) (1999) 335.
[88] J.R. Pinto, Production of Cellulose-Binding Domains by Proteolysis; Studies on the Adsorption and Modification of Cellulose Fibres, Thesis, Universidae di Minho, 2006. https://repositorium.uminho.pt/bitstream/1822/8615/1/PintoR_Tese_PhD.pdf. (Accessed 12 December 2023).
[89] International Standards Organisation, ISO, TS27687:2008, Nanotechnologies –terminology and definitions for nano-objects - nanoparticles. Nanofibre and Nanoplate Technical Specification, 2008.
[90] A. Ghazali, Y.M. Dermawan, M.R.H.M. Zukeri, R. Ibrahim, S.S. Ghazali, EFB nano fibrous cells for paper smoothing and improved printability, Adv. Mater. Res. 832 (2014), 573-542.
[91] C. Buzeo, I.I.P. Blandino, K. Robbie, Nanomaterials and nanoparticles: sources and toxicity, Biointerphases 2 (4) (2007) MR17–MR172.
[92] Q. Chaudry, Nanoparticles migration and packaging lifecycle. ILSI Europe Workshop, ilsi.Eu, 2011.
[93] Y. Song, X. Li, X. Du, Exposure to nanoparticles is related to pleural effusion, pulmonary fibrosis and granuloma, Eur. Respir. J. 34 (3) (2009) 559–567.
[94] Y. Song, X.L. Wang, Y. Rojanasakul, V. Castranova, H. Li, J. Ma, Nanomaterials in humans: identification, characteristics, and potential damage, Toxicol. Pathol. 39 (5) (2011) 841–849.
[95] Z. Zhang, Y. Yan, J. Wang, J. Song, G. Jiang, Preparation and Performance of xylan-based *Sanguisorba officinalis L.* polyphenol preservative films, New J. Chem. 33 (2023), https://doi.org/10.1039/D3NJ02796A.
[96] B.C. Guerra, S. Shahi, A. Mollaei, N. Skaf, O. Weber, F. Leite, C. Haas, Circular economy applications in the construction industry: a global scan of trends and opportunities, J. Clean. Prod. 324 (2021) 129125, https://doi.org/10.1016/j.jclepro.2021.129125.
[97] E. Mäki, H. Saastamoinen, K. Melin, D. Matschegg, H. Pihkola, Drivers and barriers in retrofitting pulp and paper industry with bioenergy for more efficient production of liquid, solid and gaseous biofuels: a review, Biomass Bioenergy 148 (2021) 106036, https://doi.org/10.1016/j.biombioe.2021.106036.
[98] Renewable Fuel Association, Essential Energy - 2021 Pocket Guide to Ethanol, 2020. https://d35t1syewk4d42.cloudfront.net/file/276/2021-Pocket-Guide.pdf#:~:text=ETHANOL%20PRODUCTION%20BY%20COUNTRY%20%28Country%2C%20million%20gallons%2C%20share,Argentina%20230%3B%201%25%20Rest%20of%20World%20500%3B%202%25.